



RESEARCH LETTER

10.1002/2015GL066636

Key Points:

- Three-dimensional Earth conductivity structure affects induced geoelectric fields
- Localized, storm time geoelectric induction could reach hazardous levels
- Improved evaluations of induction hazards require improved understanding of the solid earth

Supporting Information:

- Movie S1 caption
- Movie S1

Correspondence to:

P. A. Bedrosian,
pbedrosian@usgs.gov

Citation:

Bedrosian, P. A., and J. J. Love (2015), Mapping geoelectric fields during magnetic storms: Synthetic analysis of empirical United States impedances, *Geophys. Res. Lett.*, **42**, doi:10.1002/2015GL066636.

Received 20 OCT 2015

Accepted 20 NOV 2015

Accepted article online 25 NOV 2015

©2015. The Authors.

This is an open access article under the terms of the Creative Commons Attribution-NonCommercial-NoDerivs License, which permits use and distribution in any medium, provided the original work is properly cited, the use is non-commercial and no modifications or adaptations are made.

Mapping geoelectric fields during magnetic storms: Synthetic analysis of empirical United States impedances

Paul A. Bedrosian¹ and Jeffrey J. Love²

¹Crustal Geophysics and Geochemistry Science Center, U.S. Geological Survey, Denver, Colorado, USA, ²Geomagnetism Program, Geologic Hazards Science Center, U.S. Geological Survey, Denver, Colorado, USA

Abstract Empirical impedance tensors obtained from EarthScope magnetotelluric data at sites distributed across the midwestern United States are used to examine the feasibility of mapping magnetic storm induction of geoelectric fields. With these tensors, in order to isolate the effects of Earth conductivity structure, we perform a synthetic analysis—calculating geoelectric field variations induced by a geomagnetic field that is geographically uniform but varying sinusoidally with a chosen set of oscillation frequencies that are characteristic of magnetic storm variations. For north-south oriented geomagnetic oscillations at a period of $T_0 = 100$ s, induced geoelectric field vectors show substantial geographically distributed differences in amplitude (approximately a factor of 100), direction (up to 130°), and phase (over a quarter wavelength). These differences are the result of three-dimensional Earth conductivity structure, and they highlight a shortcoming of one-dimensional conductivity models (and other synthetic models not derived from direct geophysical measurement) that are used in the evaluation of storm time geoelectric hazards for the electric power grid industry. A hypothetical extremely intense magnetic storm having 500 nT amplitude at $T_0 = 100$ s would induce geoelectric fields with an average amplitude across the midwestern United States of about 2.71 V/km, but with a representative site-to-site range of 0.15 V/km to 16.77 V/km. Significant improvement in the evaluation of such hazards will require detailed knowledge of the Earth's interior three-dimensional conductivity structure.

1. Introduction

Geoelectric fields induced in the Earth's electrically conducting interior during geomagnetic storms [e.g., Molinski, 2002; Pirjola, 2002] can interfere with the operation of electric power grids, damage transformers, and even cause blackouts [e.g., Samuelsson, 2013; Piccinelli and Krausmann, 2014]. According to some scenarios, the future occurrence of a rare but extremely intense magnetic storm might cause widespread failure of electric power grid operations, with significant deleterious impact for society [e.g., Baker et al., 2008; Kappenman, 2012]. In the United States, this possibility has motivated the Federal Energy Regulatory Commission [FERC, 2013] (Order No. 779) to require the North American Electric Reliability Corporation to develop reliability standards to mitigate the potential impact of geomagnetic disturbances on the operation of the bulk electric power system. Concerns in the private sector have, in turn, caused reinsurance companies to make related assessments of risk [e.g., Riswadkar and Dobbins, 2010; Aon Benfield, 2013; Lloyd's, 2013].

Maps of storm time geoelectric fields could be used in a real-time setting to assess induction hazards for power grids [e.g., Bursinghaus et al., 2013; Zheng et al., 2013]; they could also be used in scenario simulations [e.g., Pulkkinen et al., 2005; Viljanen et al., 2013; Torta et al., 2014] to evaluate the vulnerability of power grids for extreme event magnetic storms [e.g., Boteler, 2001; Overbye et al., 2013]. Conceivably, regional maps of geoelectric field variation can be calculated by parameterized induction [e.g., Thomson et al., 2013; Love et al., 2014; Marti et al., 2014a]—convolving a time-dependent map of ground level geomagnetic activity with a complex impedance tensor that is a physical function of Earth conductivity. Storm time magnetic activity can be mapped by fitting parameterized functions to magnetometer data [e.g., Pulkkinen et al., 2003], thus, to some extent, filling in the geographic space between sparsely distributed observatory stations [e.g., Love and Chulliat, 2013], though more stations are certainly needed. Earth impedance represents a much bigger challenge for geoelectric mapping because the electrical conductivity of the Earth ranges across at least four orders of magnitude [e.g., Constable, 1993; Yoshino and Katsura, 2013] and because this electrical conductivity

is distributed as a complicated spatial three-dimensional function within the volume of the Earth [e.g., *Ferguson et al.*, 2012]. As a result, the induced geoelectric field variations realized at one geographic site are not always correlated with geoelectric variation at another nearby site [e.g., *McKay and Whaler*, 2006].

Magnetotelluric measurements of geomagnetic and geoelectric field variations obtained from temporary deployments of sensors at individual geographic locations [e.g., *Ferguson*, 2012] can be expressed as empirical impedance tensors [e.g., *Egbert*, 2007; *Chave*, 2012], and these, in turn, can be inverted [e.g., *Rodi and Mackie*, 2012] to obtain models of Earth conductivity [e.g., *Ferguson et al.*, 2012]. Regrettably, regional maps of storm time geoelectric field variations are often needed either where magnetotelluric surveys have not been made or where the survey sites are sparsely distributed. In some cases, estimates of Earth conductivity have been based on simplistic assumptions about stratigraphy, tectonic structure, and rock properties, and so corresponding synthetic impedance tensors are of unknown accuracy. In particular, one-dimensional, depth-dependent models of conductivity [e.g., *Ferguson and Odwar*, 1997; *Ádám et al.*, 2012; *Fernberg*, 2012] have been used to estimate storm time geoelectric fields at specific sites and within defined geographic regions [e.g., *Gannon et al.*, 2012; *Viljanen et al.*, 2013; *Wei et al.*, 2013; *Marti et al.*, 2014b]. Very recently, simulations of magnetic storm induction have been made using synthetic models of three-dimensional conductivity [e.g., *Beggan et al.*, 2013; *Beggan*, 2015], but few have used empirical impedance tensors obtained directly from magnetotelluric measurements [e.g., *McKay and Whaler*, 2006] for Scotland and England.

Recognizing a need to more fully evaluate magnetic storm induction of geoelectric fields, we use empirical impedance tensors obtained from EarthScope magnetotelluric data collected at survey sites distributed across the midwestern United States. With these tensors, we perform a synthetic analysis, calculating geoelectric fields induced by a time periodic geomagnetic field that is geographically uniform but which varies sinusoidally with a period that is representative of magnetic storm variations. Site-to-site differences in geoelectric field amplitude, direction, and temporal phase are the results of three-dimensional Earth conductivity. The results reported here are motivated, in part, by U.S. government priorities for the pursuit of scientific research that informs projects for improving the assessment and mitigation of regional, ground level space weather hazards [e.g., *NSTC*, 2015].

2. Magnetotelluric Impedance

Generally speaking, the science of magnetotellurics [e.g., *Simpson and Bahr*, 2005; *Unsworth*, 2007] is concerned with the estimation of solid-earth electrical conductivity $\sigma(\mathbf{r})$, or, equivalently, electrical resistivity $1/\sigma(\mathbf{r})=\rho(\mathbf{r})$, as a function of geographic location and depth, $\mathbf{r}=(x \text{ north}, y \text{ east}, z \text{ down})$. Analysis is made of geomagnetic $\mathbf{B}(t, x, y)$ and geoelectric $\mathbf{E}(t, x, y)$ data time series measured using sensors emplaced at locations (x, y) on the Earth's surface. It is a standard practice in mathematical treatments of the magnetotelluric problem, to reexpress field variations that are a function of time t in terms of a generalized function of frequency ω by Fourier transformation,

$$\mathcal{F}\{\mathbf{B}(t)\} = \mathbf{B}(\omega) \quad \text{and} \quad \mathcal{F}\{\mathbf{E}(t)\} = \mathbf{E}(\omega). \quad (1)$$

Many magnetotelluric analyses are focussed on just the inductional relationship between the horizontal components of the geomagnetic (B_x, B_y) and the geoelectric (E_x, E_y) fields. With this, then, geomagnetic and geoelectric field variations in an electrically conducting medium can be summarized in terms of the linear equation

$$\mathbf{E}_h(\omega, x, y) = \frac{1}{\mu} \mathbf{Z}(\omega, x, y | \sigma(\mathbf{r})) \cdot \mathbf{B}_h(\omega, x, y) \quad (2)$$

[e.g., *Weidelt and Chave*, 2012, chapter 4.1.2], where $\mathbf{Z}(\omega | \sigma(\mathbf{r}))$ is a complex impedance tensor having units of ohms (Ω) and is functionally dependent on the Earth's conductivity and μ is magnetic permeability, often assumed to be that of free space.

For a hypothetical geographic region where Earth conductivity is only a one-dimensional (1-D) function of depth [e.g., *Simpson and Bahr*, 2005, chapter 2.5], the impedance tensor is antisymmetric,

$$\mathbf{Z}(\omega | \sigma(d)) = \begin{bmatrix} 0 & Z \\ -Z & 0 \end{bmatrix} (\omega | \sigma(z)) \quad (1\text{-D}), \quad (3)$$

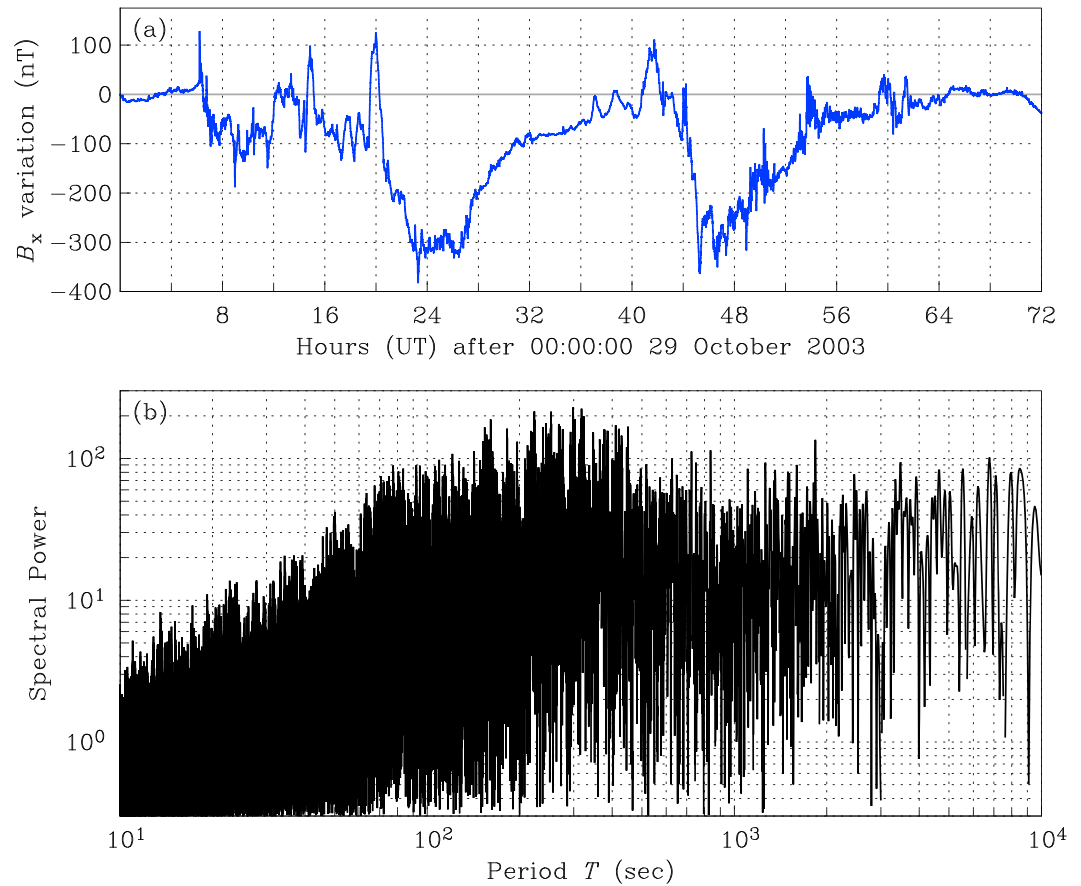


Figure 1. Data from the Memambetsu Observatory in Japan recording the Halloween magnetic storm of 29–31 October 2003: (a) three days of 1 s resolution $B_x(t)$ variation defined relative to a constant baseline and (b) Fourier spectral power of $\Delta B_x(t)$ as a function of sinusoidal period.

where each element Z is complex and frequency dependent. In this case, idealized geomagnetic variational activity that is uniform over this geographic region and aligned in one horizontal direction will induce an orthogonal geoelectric field of uniform amplitude over the region. For an even more idealized region where Earth conductivity is a half-space of uniform conductivity, geoelectric field amplitude increases as the square root of the inductive frequency, and the time-varying sinusoidal amplitude of the geoelectric field leads that of the geomagnetic field by a phase of $\pi/4$ (or $1/8$ of the inducing period). In reality, however, the sub-surface conductivity structure of the Earth (including the ocean) is three dimensional (3-D), in which case the corresponding impedance tensor is fully populated and generally asymmetric,

$$\mathbf{Z}(\omega, x, y | \sigma(\mathbf{r})) = \begin{bmatrix} Z_{xx} & Z_{xy} \\ Z_{yx} & Z_{yy} \end{bmatrix} (\omega, x, y | \sigma(\mathbf{r})) \quad (3\text{-D}), \quad (4)$$

where geographic location is denoted (x, y) and where each impedance element, for example, Z_{xx} , does not have a simple mathematical relationship to the other impedance elements, Z_{xy} , Z_{yx} , and Z_{yy} . In the case of 3-D Earth conductivity, uniform geomagnetic activity induces a geoelectric field that is geographically complicated, and at a given geographic location, induction affects the amplitude, direction, and phase of the geoelectric field in ways that cannot be realized by induction in a 1-D Earth.

3. Magnetic Storm Spectrum

Magnetic storms are transient phenomena, the causal response of the Earth's coupled magnetospheric-ionospheric system to the variable and dynamic action of the solar wind. While geomagnetic disturbance recorded at a ground-based observatory sometimes exhibits quasiperiodic variations, including pulsations

across periods of about 0.1 to 1000 s (10^{-3} to 10 Hz), storm time disturbance generally exhibits variation across a wide range of frequencies [e.g., *Olsen*, 2007]. In Figure 1a we show north component horizontal magnetic field variations $B_x(t)$ during the great Halloween storm of 29–31 October 2003 as recorded by 1 s magnetometer data from the Memambetsu Observatory (Japan Meteorological Agency, magnetic coordinates 35N, 211E); note the occasional impulsive variations, as well as periods of rapid oscillation. In Figure 1b we show the corresponding Fourier domain frequency (period) power spectrum calculated from first differences in time of the north geomagnetic field component $\Delta B_x = B_x(t_i) - B_x(t_{i-1})$. Spectral power is distributed across a broad wash of periods with maximum spectral power at about $2\pi/\omega_0 = T_0 = 300$ s, though it is important to recognize that, in general, every magnetic storm time series has its own unique power spectrum. Note that electric utility companies, in their evaluation of the vulnerability of high-voltage power grid transformers, are concerned with geomagnetic field variations occurring across periods of about 10 to 1000 s (about 10^{-3} to 10^{-1} Hz) [e.g., *Barnes et al.*, 1991; *NERC*, 2014a, 2014b].

4. Earthscope Impedance Tensors

Since 2006, the EarthScope USArray program of the National Science Foundation [*Williams et al.*, 2010] has supported magnetotelluric surveys over large geographic parts of the United States [*Schultz*, 2009]. These surveys were accomplished by temporary 3 week deployments of electromagnetic measurement systems at individual locations (x_i, y_i) having nominal 70 km spacing. At each site, 1 Hz geomagnetic field vector data were collected using a fluxgate magnetometer; simultaneously, 1 Hz horizontal component geoelectric field vector data were collected using two orthogonal pairs of nonpolarizable lead-lead chloride electrodes planted into the ground. Data from each measurement site have been used to estimate an empirical magnetotelluric impedance tensor $\mathbf{Z}^e(\omega, x_i, y_i)$ [*Egbert*, 2007]; most of these tensors are well defined for periods of about 10 to 10,000 s (10^{-4} to 10^{-1} Hz) with errors generally estimated to be 5% or less. These tensors, in turn, have been used to estimate Earth conductivity models for the United States [e.g., *Bedrosian and Feucht*, 2014; *Meqbel et al.*, 2014; *Yang et al.*, 2015]. During the EarthScope magnetotelluric campaign of 2011–2014, 305 station deployments were made across the north midwestern United States; seven stations were determined to be of poor data quality at the period of primary interest and were excluded from the following analysis. We use those impedance tensors in this analysis; the locations of the 298 stations used are shown in Figure 2 (to which we will return in section 6).

5. Synthetic Forward Problem

At each magnetotelluric survey site (x_i, y_i) , it is straightforward to describe the inductive relationship between geomagnetic and geoelectric field variations using the empirically derived impedance tensor,

$$\mathbf{E}_h(\omega, x_i, y_i) = \frac{1}{\mu} \mathbf{Z}^e(\omega, x_i, y_i) \cdot \mathbf{B}_h(\omega, x_i, y_i). \quad (5)$$

So as to isolate the effects of solid-earth electrical conductivity structure, we assume that the inducing geomagnetic field is simple and geographically uniform, varying in time as a sinusoid,

$$\mathbf{B}_h(t) = \mathbf{B}_h(\omega_0) \exp(-i\omega_0 t), \quad (6)$$

where $\mathbf{B}_h(\omega_0)$ is a time constant vector, $\omega_0 = 2\pi/T_0$ is a fixed frequency, and $i = \sqrt{-1}$. In the Fourier-transformed frequency domain,

$$\mathcal{F}\{\mathbf{B}_h(t)\} = \mathbf{B}_h(\omega_0) \delta(\omega - \omega_0), \quad (7)$$

where $\delta(\omega)$ is the Dirac delta function. The corresponding synthetic geoelectric vector is given by

$$\mathbf{E}_h(\omega, x_i, y_i) = \frac{1}{\mu} \mathbf{Z}^e(\omega, x_i, y_i) \cdot \mathbf{B}_h(\omega_0) \delta(\omega - \omega_0). \quad (8)$$

This can be expressed as a sinusoidal variation after inverse Fourier transformation,

$$\mathcal{F}^{-1}\{\mathbf{E}_h(\omega)\} = \mathbf{E}_h(t), \quad (9)$$

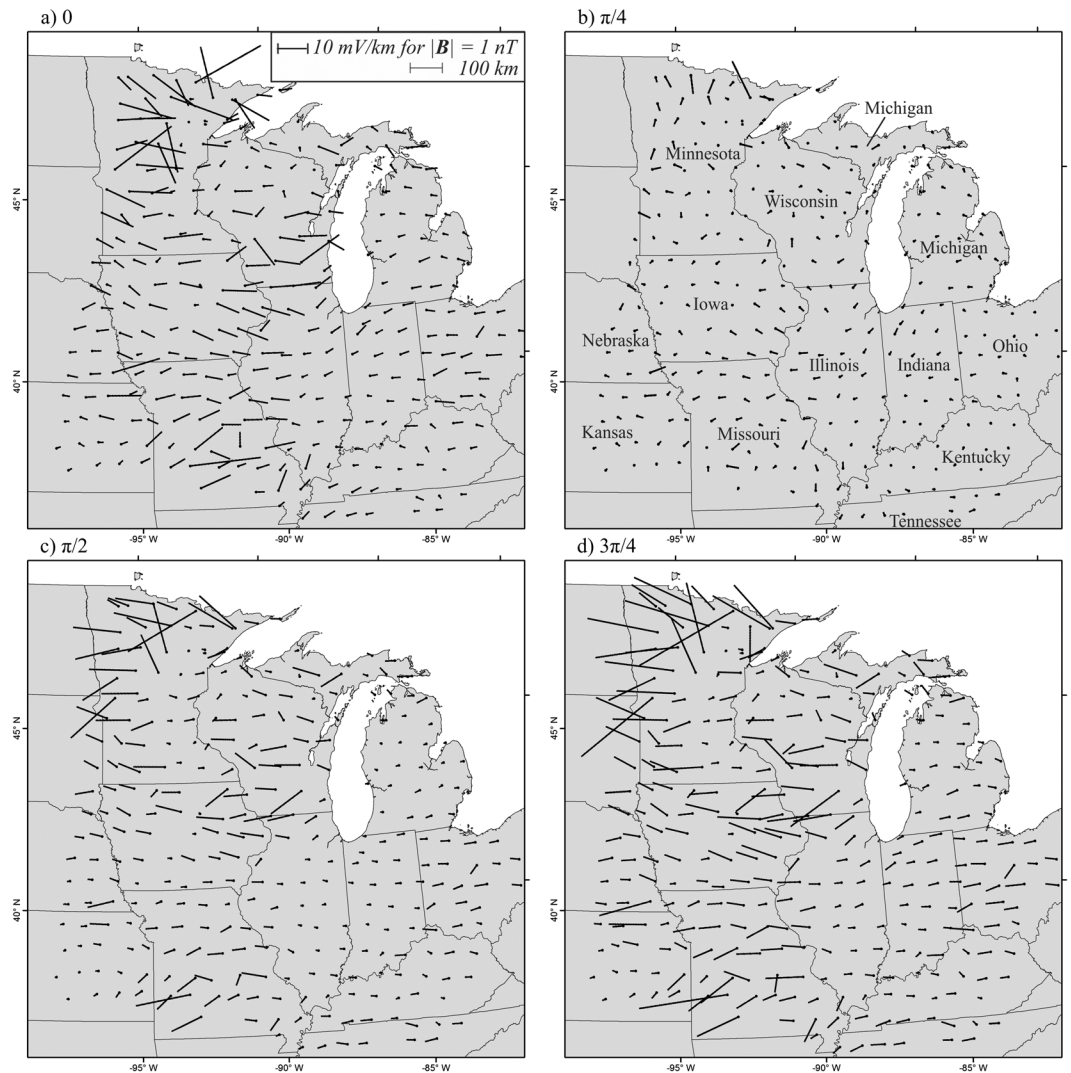


Figure 2. The oscillation of horizontal geoelectric field vectors $\mathbf{E}_h(t)$ (black) at four different instances in time, (a) $t=0$, (b) $t=\frac{1}{4}\pi/\omega_0$, (c) $t=\frac{2}{4}\pi/\omega_0$, and (d) $t=\frac{3}{4}\pi/\omega_0$, as induced by a 1 nT amplitude, north-south $B_x(t)$, geomagnetic field sinusoid having a $T_0 = 100$ s period. The corresponding geoelectric field amplitudes range from 0.30 mV/km (EarthScope RED36) to 33.55 mV/km (MNB36), and among the sites shown, the mean is 5.43 mV/km. Geoelectric field directions range over 130° .

so that

$$\mathbf{E}_h(t, x_i, y_i) = \mathbf{E}_h(\mathbf{Z}^e, \mathbf{B}_h) \exp(-i\omega_0 t). \quad (10)$$

6. Time Series and Maps

In Figure 2 we show, for each EarthScope survey site, maps corresponding to four discrete instances, $t = \frac{n}{4}\pi/\omega_0$ for $n = 0, 1, 2, 3$ in the sinusoidal time dependence of horizontal geoelectric vectors $\mathbf{E}_h(t)$ (black) that are induced by a synthetic north-south $B_x(t)$ geomagnetic field sinusoid with $T_0 = 100$ s (10^{-2} Hz) and 1 nT amplitude; compare these maps with those of McKay and Whaler [2006, Figure 3] for southern Scotland and northern England. The time progression of the geoelectric field vectors is also available as Movie S1 in the supporting information. Figure 2b shows geoelectric field amplitudes near their minimum, and Figure 2d shows amplitudes near their maximum. From these maps we see that in some areas, such as across central Indiana, geoelectric field amplitudes are relatively uniform—there is relatively little difference from one survey site to its ~ 70 km neighbor, and geoelectric field directions at some sites are close to being east-west oriented and, thus, orthogonal to the north-south inducing geomagnetic field. Such properties are consistent with

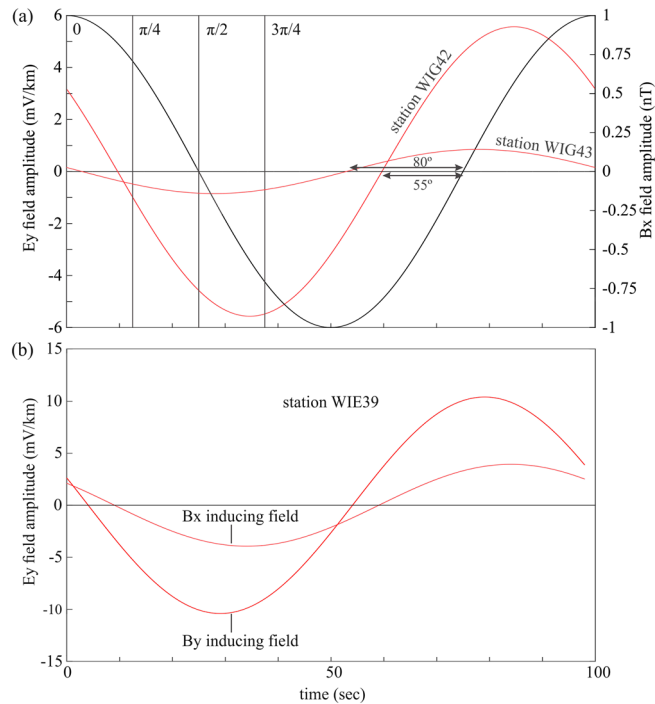


Figure 3. (a) East-west geoelectric field components $E_y(t)$ (red) induced at two adjacent sites in northeastern Wisconsin (EarthScope WIG42 and WIG43) separated by ~ 70 km and induced by a synthetic, $T_0 = 100$ s, 1 nT amplitude geomagnetic field sinusoid $B_x(t)$ (black). (b) East-west geoelectric field component $E_y(t)$ (red) induced at a single site in northern Wisconsin (EarthScope WIE39) by north-south $B_x(t)$ and east-west $B_y(t)$ field.

those for Earth conductivity that is locally 1-D for induction at 10^{-2} Hz. Otherwise, across most of the regions shown in Figure 2, there is substantial geographic variation in both the amplitude and direction of the geoelectric field; this is most dramatic in Minnesota, where geoelectric field amplitudes range from 0.30 mV/km to 33.55 mV/km, and differences between the geoelectric directions range over 130° . That the induced geoelectric field vectors are not everywhere of uniform amplitude, nor everywhere uniformly aligned in the east-west direction, are clear indications of 3-D Earth conductivity structure.

In Figure 3a, we compare the east-west geoelectric field components $E_y(t)$ (red) induced by a synthetic, $T_0 = 100$ s, 1 nT amplitude geomagnetic field sinusoid $B_x(t)$ (black) for two survey sites separated by just 70 km in northeastern Wisconsin. Between the two sites, geoelectric field amplitudes differ by nearly a factor of 10. The geoelectric field sinusoids are seen to lead the geomagnetic field sinusoid but not exactly by the $\pi/4$ or 45° phase that would be expected for a uniformly conducting half-space; instead, phases of 55° and 80° are observed, corresponding to a difference in time of nearly 7 s between these two neighboring sites. In Figure 3b we compare the east-west field geoelectric field component $E_y(t)$ for north-south inducing $B_x(t)$ and east-west inducing $B_y(t)$, each at a single site in northern Wisconsin. Note that amplitudes of the induced geoelectric fields differ by more than a factor of 2 solely as the result of the direction of the inducing geomagnetic field; this is an effect caused by 3-D Earth conductivity.

In Figure 4, we compare geoelectric field vectors $\mathbf{E}_h(t)$ for north-south $B_x(t)$ inducing geomagnetic field sinusoids having three different periods, $T_0 = 10, 100, 1000$ s (red, black, and green), each at $t = \frac{3}{4}\pi/\omega_0$. While the red vectors are usually longer than the black vectors which are longer than the green vectors, differences in amplitude ratios exist from one site to another; in general, amplitude does not increase as the square root of frequency, as would be expected for a uniformly conducting half-space. We note that geoelectric field direction is also a function of the frequency; at some sites the red, black, and green vectors are not parallel; this is an effect of 3-D Earth conductivity.

In Figure 5, we compare geoelectric field vectors $\mathbf{E}_h(t)$ induced by a $T_0 = 100$ s, north-south $B_x(t)$ geomagnetic field sinusoid (black) and east-west $B_y(t)$ sinusoid (red), in each case at $t = \frac{3}{4}\pi/\omega_0$. In some areas, such as across central Indiana, geoelectric field vectors are nearly orthogonal to the direction of the geomagnetic field,

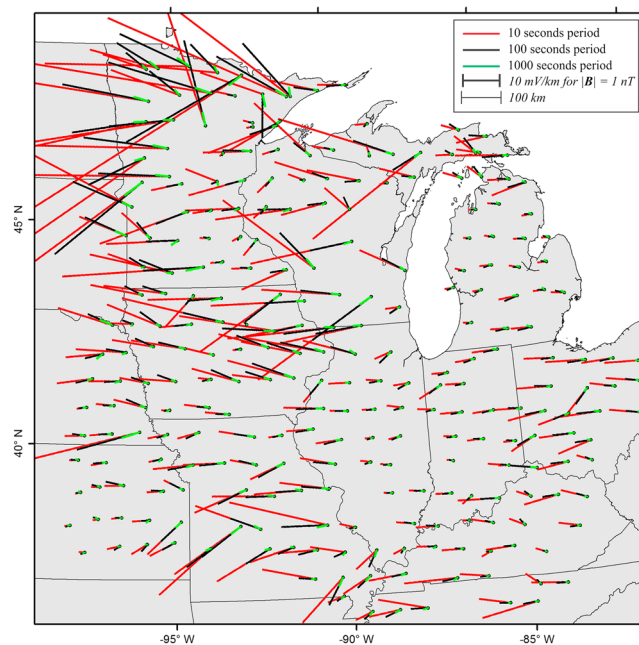


Figure 4. Horizontal geoelectric field vectors $\mathbf{E}_h(t)$ at $t = \frac{3}{4}\pi/\omega_0$ induced by a north-south $B_x(t)$ geomagnetic field sinusoid, having 10 s (red), 100 s (black), and 1000 s (green) periods. For geomagnetic field variation having 1 nT amplitude, the respective geoelectric field amplitudes range from 1.21 mV/km (EarthScope REE36) to 79.00 mV/km (MNB36), 0.30 mV/km (RED36) to 33.55 mV/km (MNB36), and 0.05 mV/km (IAK38) to 6.03 mV/km (MOS39).

and they have nearly the same amplitude regardless of the direction of the inducing geomagnetic field, as would be expected for Earth conductivity that is locally 1-D for induction at 10^{-2} Hz. In other areas, the effects of 3-D Earth conductivity are clearly seen. For example, at some sites in northern Minnesota and northern Wisconsin, geoelectric field amplitudes induced by east-west geomagnetic field variation are substantially greater than those induced by north-south geomagnetic field variation, as also seen in Figure 3b;

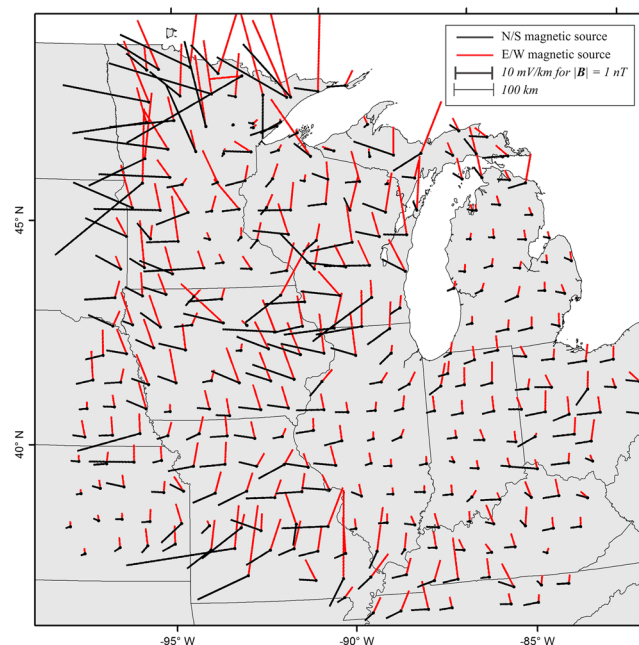


Figure 5. Horizontal geoelectric vectors $\mathbf{E}_h(t)$ at $t = \frac{3}{4}\pi/\omega_0$ induced by a geomagnetic sinusoid having a $T_0 = 100$ s period that is oriented north-south $B_x(t)$ (black) and east-west $B_y(t)$ (red).

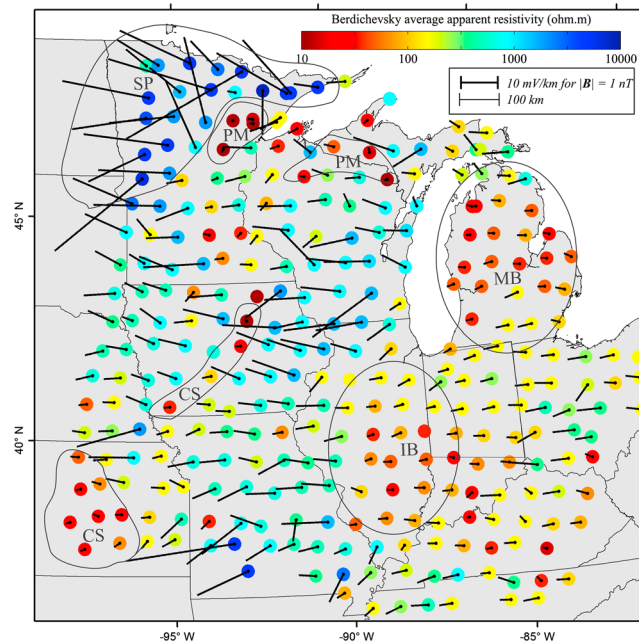


Figure 6. Berdichevsky apparent resistivity for $T_0 = 100$ s and geoelectric field vectors $\mathbf{E}_h(t)$ for a north-south $B_x(t)$ inducing geomagnetic field at $t = \frac{3}{4}\pi/\omega_0$. Thin black outlines denote the geologic extent of features discussed in the text. Illinois Basin (IB), Michigan Basin (MB), Paleoproterozoic metasediments (PM), rift sediments (CS), and Superior province (SP).

in other areas, the opposite relationship is seen. Some sites show evidence of current channeling [e.g., *Simpson and Bahr*, 2005, chapter 5.9], with some geoelectric field vectors oriented at acute angles and others at obtuse angles relative to the direction of the inducing geomagnetic field.

7. Resistivity and Geological Interpretations

As a distillation of the impedance tensor down to a scalar function of frequency, allowing us to relate our geoelectric field estimates to a data-based proxy for Earth resistivity, we calculate the Berdichevsky (or Berdichevskiy) apparent resistivity from the principal (off-diagonal) elements of the EarthScope empirical impedance tensors for $T_0 = 100$ s,

$$\rho^B(\omega_0, x_i, y_i) = \frac{1}{4\mu\omega_0} \left| Z_{xy}^e - Z_{yx}^e \right|^2 \quad (11)$$

[*Berdichevskiy and Dmitriev*, 1976; *Simpson and Bahr*, 2005, chapter 8.4]. We show these Berdichevsky apparent resistivities in Figure 6 as colored circles at each of the survey sites; most of the ρ^B values fall in a range from 10 to $10^3 \Omega \cdot \text{m}$. Their corresponding electromagnetic skin depths

$$\delta \approx \sqrt{\frac{\rho T}{\pi \mu}} \quad (12)$$

range from about 15 km down to about 150 km. But magnetotelluric induction is most sensitive to resistivity structure at a fraction of a skin depth, with a rule of thumb being $\delta/10$. Hence, the ρ^B values shown in Figure 6 are probably reflecting subsurface structure at depths of 1.5–15 km. Geographic variations in ρ^B are correlated with the magnitude of geoelectric field vectors: larger field amplitudes are associated with areas of higher ρ^B (more resistive) while more attenuated field amplitudes are associated with lower values of ρ^B (more conductive).

We can interpret Figure 6 in terms of the geological history of North America [e.g., *Bally and Palmer*, 1989] and in the context of fully developed 3-D Earth conductivity models for the north midwestern United States [e.g., *Yang et al.*, 2015; P. A. Bedrosian, Making it and breaking it in the Midwest: Continental assembly and

rifting from modeling of EarthScope magnetotelluric data, submitted to *Precambrian Research*, 2015]. High-amplitude geoelectric fields and Berdichevsky ρ^B in northern Minnesota correspond to the Archean Superior province (Figure 6, SP), old and cold rocks that are largely devoid of electrically conducting mineral phases. In contrast, deep intracontinental basins, such as the Michigan and Illinois Basins (MB and IB), are filled with conductive sedimentary rocks, resulting in lower ρ^B values and smaller geoelectric field amplitudes. Some of the most abrupt site-to-site differences in geoelectric field amplitudes, such as in northern Minnesota and northern Wisconsin, correspond to ancient faults and suture zones which juxtapose resistive igneous and metamorphic basement against Paleoproterozoic metasedimentary rocks (PM) containing electrically conductive metallic sulfides and graphite. Similar variations in amplitude are also observed in Iowa and Kansas, where clastic sediments (CS) shed from the Mesoproterozoic Midcontinent Rift System are juxtaposed against thick sequences of resistive volcanic and intrusive rocks. The configuration of these sedimentary basins is reflected in Figure 6 as areas of lower ρ^B and smaller geoelectric field amplitudes adjacent to areas of higher ρ^B values and geoelectric field amplitudes.

8. Implications for Hazard Assessments

The preceding analysis, made using empirical impedance tensors derived directly from measurement, demonstrates that the effect of 3-D Earth conductivity structure is a factor of primary importance in the induction of geoelectric fields during magnetic storms. By corollary, impedance tensors estimated from simplistic 1-D depth-dependent Earth conductivity models that have not been validated against direct geoelectric field measurements can lead to estimates that are extremely inaccurate; for example, a 1-D model for Minnesota would give geoelectric field amplitudes that are erroneous by about a factor of 100 and errors in the direction of the geoelectric field of up to 130°. As egregious as such errors might seem, they follow from the assumption that the inducing geomagnetic field is geographically uniform. Of course, storm time geomagnetic activity can have a complicated and sometimes very localized geographic realization across the Earth's surface [e.g., *Pulkkinen et al.*, 2006; *Ngwira et al.*, 2015]. And so the convolution of geographically realistic geomagnetic activity through the impedance of realistic 3-D solid-earth and ocean will, in general, give rise to induced geoelectric fields that have a geographic complexity even greater than that shown in our synthetic analysis.

In more specific terms, a hypothetical extremely intense magnetic storm having 500 nT amplitude at period of $T_0 = 100$ s, which is plausible [e.g., *Thomson et al.*, 2011], would induce geoelectric fields with an average amplitude of about 2.71 V/km but a representative site-to-site range of 0.15 V/km to 16.77 V/km. The average for such a hypothetical event is similar to the 100 year benchmark event that is being used by the electric power grid industry in the United States to guide magnetic storm mitigation efforts [NERC, 2014a]. However, the site-to-site range in geoelectric amplitude, the result of 3-D Earth conductivity structure, is substantially greater than that inferred from those simple 1-D and synthetic 3-D conductivity models. Power grids that are deployed across geographically complex Earth conductivity will have geomagnetically induced currents that are proportional to a corresponding geographic average of the induced geoelectric field. In general, if the average geoelectric field is to be accurately calculated, localized geoelectric fields need to be accurately estimated. To improve the accuracy, we conclude that reliable evaluations of induction hazards at the Earth's surface, generated by space weather processes above the Earth, require much more detailed knowledge of the 3-D conductivity structure of the Earth's interior.

References

- Ádám, A., E. Prácer, and V. Wessztergom (2012), Estimation of the electric resistivity distribution (EURHOM) in the European lithosphere in the frame of the EURISGIC WP2 Project, *Acta Geod. Geoph. Hung.*, 47, 377–387, doi:10.1556/AGeod.47.2012.4.1.
- Aon Benfield (2013), *Geomagnetic Storms*, pp. 1–12, Aon Benfield, Sydney, Australia.
- Baker, D. N., et al. (2008), *Severe Space Weather Events—Understanding Societal and Economic Impacts*, pp. 1–144, National Academy Press, Washington, D. C.
- Bally, A. W., and A. R. Palmer (1989), *The Geology of North America: An Overview*, pp. 1–629, Geol. Soc. Am., Boulder, Colo., doi:10.1130/DNAG-GNA-A.
- Barnes, P. R., D. T. Rizy, B. W. McConnell, F. M. Tesche, and E. R. Taylor Jr. (1991), *Electric Utility Industry Experience With Geomagnetic Disturbances*, vol. ORNL–6665, 1–78 pp., Oak Ridge Natl. Lab.
- Bedrosian, P. A., and D. W. Feucht (2014), Structure and tectonics of the northwestern United States from EarthScope USArray magnetotelluric data, *Earth Planet. Sci. Lett.*, 402, 275–289, doi:10.1016/j.epsl.2013.07.035.
- Beggan, C. D. (2015), Sensitivity of geomagnetically induced currents to varying auroral electrojet and conductivity models, *Earth Planets Space*, 67, 24, doi:10.1186/s40623-014-0168-9.
- Beggan, C. D., D. Beamish, A. Richards, G. S. Kelly, and A. W. P. Thomson (2013), Prediction of extreme geomagnetically induced currents in the UK high-voltage network, *Space Weather*, 11, 407–419, doi:10.1002/swe.20065.

Acknowledgments

We thank C.A. Finn, A. Kelbert, J. McCarthy, and J.L. Slate for reviewing a draft manuscript. We thank E.J. Rigler for useful conversations. This work would not have been possible without the efforts of the National Geoelectromagnetic Facility at Oregon State University, Zonge Engineering and Research Organization, and Green Geophysics, all of whom oversaw or carried out the acquisition of the EarthScope MT data presented here. A. Schultz, G.D. Egbert, and A. Kelbert are particularly thanked for the data QA/QC and time series analysis which make this data set accessible to the Earth science community. This work was supported by the USGS Geomagnetism Program. Magnetometer data from the Memambetsu Observatory can be obtained from either the Kakioka magnetic observatory (www.kakioka-jma.go.jp) or the Kyoto World Data Center (<http://wdc.kugi.kyoto-u.ac.jp>). EarthScope magnetotelluric impedance tensors can be obtained from the Data Management Center of the Incorporated Research Institutions for Seismology (ds.iris.edu/ds/products/emtf). Any use of trade, firm, or product names is for descriptive purposes only and does not imply endorsement by the U.S. Government.

- Berdichevskiy, M. N., and V. I. Dmitriev (1976), Distortion of magnetic and electrical fields by near-surface lateral inhomogeneities, *Acta Geodaet. Geophys. Montanist. Acad. Sci. Hung.*, *11*, 447–483.
- Boteler, D. H. (2001), Assessment of geomagnetic hazard to power systems in Canada, *Nat. Hazards*, *23*, 101–120.
- Burstinghaus, E. J., T. K. Saha, R. A. Marshall, and K. Yumoto (2013), The importance of non-uniform geoelectric fields in calculating GIC distributions, in *Power and Energy Society General Meeting (PES)*, pp. 1–5, IEEE, Vancouver, B. C., doi:10.1109/PESMG.2013.6672289
- Chave, A. D. (2012), Estimation of the magnetotelluric response function, in *The Magnetotelluric Method*, edited by A. D. Chave and A. G. Jones, pp. 165–218, Cambridge Univ. Press, Cambridge, U. K.
- Constable, S. C. (1993), Constraints on mantle electrical conductivity from field and laboratory measurements, *J. Geomag. Geoelectr.*, *45*, 707–728.
- Egbert, G. D. (2007), Robust electromagnetic transfer functions estimates, in *Encyclopedia of Geomagnetism and Paleomagnetism*, edited by D. Gubbins and E. Herrero-Bervera, pp. 866–870, Springer, Dordrecht, Netherlands.
- FERC (2013), Reliability standards for geomagnetic disturbances, *Fed. Energy Reg. Comm. Fed. Reg. Rules Regulations*, *78*(100), 30,747–30,762.
- Ferguson, I. J. (2012), Instrumentation and field procedure, in *The Magnetotelluric Method*, edited by A. D. Chave and A. G. Jones, pp. 421–479, Cambridge Univ. Press, Cambridge, U. K.
- Ferguson, I. J., and H. D. Odwar (1997), Review of conductivity soundings in Canada, Appendix 3, in *Geomagnetically Induced Currents: Geomagnetic Hazard Assessment, Phase II, 357 T 848A*, vol. 3, edited by D. H. Boteler, pp. 1–121, Geol. Surv. Canada and Canadian Electr. Assoc.
- Ferguson, I. J., A. G. Jones, and A. D. Chave (2012), Case histories and geological applications, in *The Magnetotelluric Method*, edited by A. D. Chave and A. G. Jones, pp. 480–544, Cambridge Univ. Press, Cambridge, U. K.
- Fernberg, P. (2012), *One-Dimensional Earth Resistivity Models for Selected Areas of Continental United States and Alaska*, pp. 1–190, EPRI Technical Update 1026430, Palo Alto, Calif.
- Gannon, J. L., L. Trichtchenko, and P. Fernberg (2012), United States regional GIC hazard assessment, Abstract SM21D-08 presented at 2012 Fall Meeting, AGU, San Francisco, Calif., 3–7 Dec.
- Kappenman, J. G. (2012), A perfect storm of planetary proportions, *49*.
- Lloyd's (2013), *Emerging Risk Report: Solar Storm Risk to the North American Electric Grid*, pp. 1–22, Lloyd's of London, London, U. K.
- Love, J. J., and A. Chulliat (2013), An international network of magnetic observatories, *Eos Trans. AGU*, *94*(42), 373–384, doi:10.1002/2013EO420001.
- Love, J. J., E. J. Rigler, A. Pulkkinen, and C. C. Balch (2014), Magnetic storms and induction hazards, *Eos Trans. AGU*, *95*(48), 445–446, doi:10.1002/2014EO480001.
- Marti, L., A. Rezaei-Zare, and D. Boteler (2014a), Calculation of induced electric field during a geomagnetic storm using recursive convolution, *IEEE Trans. Power Delivery*, *29*, 802–807, doi:10.1109/TPWRD.2013.2273833.
- Marti, L., C. Yiu, A. Rezaei-Zare, and D. Boteler (2014b), Simulation of geomagnetically induced currents with piecewise layered-Earth models, *IEEE Trans. Power Delivery*, *29*, 1186–1193, doi:10.1109/TPWRD.2014.2317851.
- McKay, A. J., and K. A. Whaler (2006), The electric field in northern England and southern Scotland: Implications for geomagnetically induced currents, *Geophys. J. Int.*, *167*, 613–625, doi:10.1111/j.1365-246X.2006.03128.x.
- Meqbel, N. M., G. D. Egbert, P. E. Wannamaker, A. Kelbert, and A. Schultz (2014), Deep electrical resistivity structure of the northwestern U.S. derived from 3-D inversion of USArray magnetotelluric data, *Earth Planet. Sci. Lett.*, *402*, 290–304, doi:10.1016/j.epsl.2013.12.026.
- Molinski, T. S. (2002), Why utilities respect geomagnetically induced currents, *J. Atmos. Sol. Terr. Phys.*, *64*, 1765–1778.
- NERC (2014a), *Benchmark Geomagnetic Disturbance Event Description*, pp. 1–26, North Am. Electric Reliability Corp., Atlanta, Ga.
- NERC (2014b), *Transformer Thermal Impact Assessment: Project 2013-03 (Geomagnetic Disturbance Mitigation)*, pp. 1–16, North Am. Electric Reliability Corp., Atlanta, Ga.
- Ngwira, C. M., A. A. Pulkkinen, E. Bernabeu, J. Eichner, A. Viljanen, and G. Crowley (2015), Characteristics of extreme geoelectric fields and their possible causes: Localized peak enhancements, *Geophys. Res. Lett.*, *42*, 6916–6921, doi:10.1002/2015GL065061.
- NSTC (2015), *National Space Weather Strategy*, pp. 1–13, Executive Office, National Sci. Tech. Council, Washington, D. C.
- Olsen, N. (2007), Natural sources for electromagnetic induction studies, in *Encyclopedia of Geomagnetism and Paleomagnetism*, edited by D. Gubbins and E. Herrero-Bervera, pp. 743–746, Springer, Dordrecht, Netherlands.
- Overbye, T. J., K. S. Shetye, T. R. Hutchins, Q. Qiu, and J. D. Weber (2013), Power grid sensitivity analysis of geomagnetically induced currents, *IEEE Trans. Power Syst.*, *28*, 4821–4828, doi:10.1109/TPWRS.2013.2274624.
- Piccinelli, R., and E. Krausmann (2014), *Space Weather and Power Grids—A Vulnerability Assessment*, pp. 1–53, European Union, Luxembourg.
- Pirjola, R. (2002), Review on the calculation of surface electric and magnetic fields and of geomagnetically induced currents in ground-based technological systems, *Surv. Geophys.*, *23*, 71–90.
- Pulkkinen, A., O. Amm, A. Viljanen, and BEAR Working Group (2003), Separation of the geomagnetic variation field on the ground into external and internal parts using the spherical elementary current system, *Earth Planets Space*, *55*, 117–129.
- Pulkkinen, A., S. Lindahl, A. Viljanen, and R. Pirjola (2005), Geomagnetic storm of 29–31 October 2003: Geomagnetically induced currents and their relation to problems in the Swedish high-voltage power transmission system, *Space Weather*, *3*, S08C03, doi:10.1029/2004SW000123.
- Pulkkinen, A., A. Klimas, D. Vassiliadis, V. Uritsky, and E. Tanskanen (2006), Spatiotemporal scaling properties of the ground geomagnetic field variations, *J. Geophys. Res.*, *111*, A03305, doi:10.1029/2005JA011294.
- Riswadkar, A. V., and B. Dobbins (2010), *Solar Storms: Protecting Your Operations Against the Sun's "Dark Side"*, pp. 1–12, Zurich Services Corp., Schaumburg, Ill.
- Rodi, W. L., and R. L. Mackie (2012), The inverse problem, in *The Magnetotelluric Method*, edited by A. D. Chave and A. G. Jones, pp. 347–420, Cambridge Univ. Press, Cambridge, U. K.
- Samuelsson, O. (2013), *Geomagnetic Disturbances and Their Impact on Power Systems*, pp. 1–18, Ind. Elec. Eng. Auto., Lund Univ., Lund, Sweden.
- Schultz, A. (2009), A continental scale magnetotelluric observatory and data discovery resource, *Data Sci. J.*, *8*, IGY6–IGY20.
- Simpson, F., and K. Bahr (2005), *Practical Magnetotellurics*, pp. 1–254, Cambridge Univ. Press, Cambridge, U. K.
- Thomson, A. W. P., A. J. McKay, and A. Viljanen (2009), A review of progress in modelling of induced geoelectric and geomagnetic fields with special regard to induced currents, *Acta Geophys.*, *57*, 209–219.
- Thomson, A. W. P., E. B. Dawson, and S. J. Reay (2011), Quantifying extreme behavior in geomagnetic activity, *Space Weather*, *9*, S10001, doi:10.1029/2011SW000696.
- Torta, J. M., S. Marsal, and M. Quintana (2014), Assessing the hazard from geomagnetically induced currents to the entire high-voltage power network in Spain, *Earth Planets Space*, *66*, 87, doi:10.1186/1880-5981-66-87.

- Unsworth, M. (2007), Magnetotellurics, in *Encyclopedia of Geomagnetism and Paleomagnetism*, edited by D. Gubbins and E. Herrero-Bervera, pp. 670–673, Springer, Dordrecht, Netherlands.
- Viljanen, A., R. Pirjola, E. Prácser, S. Ahmadzai, and V. Singh (2013), Geomagnetically induced currents in Europe: Characteristics based on a local power grid model, *Space Weather*, *11*, 575–584, doi:10.1002/swe.20098.
- Wei, L. H., N. Homeier, and J. L. Gannon (2013), Surface electric fields for North America during historical geomagnetic storms, *Space Weather*, *11*, 451–462, doi:10.1002/swe.20073.
- Weidelt, P., and A. D. Chave (2012), The magnetotelluric response function, in *The Magnetotelluric Method*, edited by A. D. Chave and A. G. Jones, pp. 122–164, Cambridge Univ. Press, Cambridge, U. K.
- Williams, M. L., et al. (2010), *Unlocking the Secrets of the North American Continent: An EarthScope Science Plan for 2010–2020*, pp. 1–78, EarthScope.
- Yang, B., G. D. Egbert, A. Kelbert, and N. M. Meqbel (2015), Three-dimensional electrical resistivity of the north-central USA from EarthScope long period magnetotelluric data, *Earth Planet. Sci. Lett.*, *422*, 87–93.
- Yoshino, T., and T. Katsura (2013), Electrical conductivity of mantle minerals: Role of water in conductivity anomalies, *Ann. Rev. Earth Planet. Sci.*, *41*, 605–628.
- Zheng, K., L. Trichtchenko, R. Pirjola, and L. G. Liu (2013), Effects of geophysical parameters on GIC illustrated by benchmark network modeling, *IEEE Trans. Power Delivery*, *28*, 1183–1191, doi:10.1109/TPWRD.2013.2249119.